Nuclear Medicine and Biology 144–145 (2025) 109011

Contents lists available at ScienceDirect

Nuclear Medicine and Biology

journal homepage: www.elsevier.com/locate/nucmedbio

Radiation dosimetry of the 18 kDa translocator protein ligand [^{18}F]PBR111 in humans

Benjamin B. Tournier [a,b], Zahra Mansouri [c], Yazdan Salimi [c], Kelly Ceyzériat [d], Gregory Mathoux [c], Hélène Richard-Lepouriel [e], Daniel Zullino [a,f], Frédéric Bois [c], Habib Zaidi [a,c], Valentina Garibotto [a,c], Stergios Tsartsalis [a,e,1], Philippe Millet [a,b,*,1]

[a] Faculty of Medicine, University of Geneva, Geneva, Switzerland
[b] Department of Psychiatry, University Hospitals of Geneva, Geneva, Switzerland
[c] Diagnostic Department, Division of Nuclear Medicine and Molecular Imaging, University Hospitals of Geneva, Geneva, Switzerland
[d] CIBM Center for Biomedical Imaging, Geneva, Switzerland
[e] Department of Psychiatry, Mood and Anxiety Disorders Unit, University Hospitals of Geneva, Geneva, Switzerland
[f] University Hospitals of Geneva, Geneva, Switzerland

ARTICLE INFO

Keywords:
PBR
TSPO
Radiation dose

ABSTRACT

Purpose: The 18 kDa translocator protein (TSPO) is a mitochondrial protein that becomes overexpressed during neuroinflammatory conditions, such as in Alzheimer's disease or multiple sclerosis. TSPO is of interest because it serves as a marker for microglial and astrocytic activity, measurable via in vivo positron emission tomography (PET) molecular imaging. [^{18}F]PBR111 is a second-generation TSPO PET radioligand with high signal specificity but a sensitivity to TSPO polymorphism, in comparison with first-generation ligands. This study focused on the biodistribution and dosimetry of [^{18}F]PBR111 in healthy humans.

Method: Six volunteers (three males, three females) were administered approximately 200 MBq of [^{18}F]PBR111. Organs such as the lungs and liver showed the highest initial radioactivity level, while the bone marrow and bladder accumulated activity over time, likely reflecting ligand defluorination and elimination.

Results: Dosimetry findings revealed a total effective dose of 16.17 μSv/MBq, equivalent to 3.04 mSv per examination. Compared to animal models, human dosimetry showed lower radiation exposure, highlighting discrepancies in predictive models. Organ-specific dose comparisons with other TSPO ligands ([^{18}F]PBR06, [^{18}F]FEPPA, [^{18}F]FEDAA1106) revealed similar distribution patterns. This study underscores the clinical viability of [^{18}F]PBR111 for TSPO imaging, providing critical data for optimizing its safe use in research and clinical settings.

Conclusion: The findings support its potential for studying neuroinflammatory and systemic diseases. The trial registration number is NCT06398392.

1. Introduction

The 18 kDa translocator protein (TSPO) is a mitochondrial protein whose functions and roles in the brain remain incompletely understood. It is expressed by microglial cells, astrocytes, endothelial cells, and even some neurons and other cell types [1–3]. However, in the event of a neuroinflammatory reaction, TSPO density has been demonstrated to increase. Indeed, in mouse models of multiple sclerosis, astrocytes and microglia have been observed to overexpress TSPO at varying stages of the pathology [4–6]. In a rat model of Alzheimer's disease (AD), TSPO is only overexpressed by astrocytes at the onset of pathology, followed by astrocytes and microglia [7]. In the human brain, increases of the TSPO signal from astrocytes and microglial cell populations were observed in the context of AD [7,8]. The over-expression of TSPO was also observed in other pathologies (Parkinson's disease, stroke, amyotrophic lateral sclerosis, epilepsy…) [9,10]. In schizophrenia, however, there is no consensus on the increase in TSPO density [10–12]. The origin of the increase in TSPO could depend on cell type and animal species, and

* Corresponding author at: University Hospitals of Geneva, Department of Psychiatry, Avenue de la Roseraie, 64, 1205 Geneva, Switzerland.
E-mail address: philippe.millet@hcuge.ch (P. Millet).
[1] These authors jointly supervised this work.

https://doi.org/10.1016/j.nucmedbio.2025.109011
Received 16 December 2024; Received in revised form 12 March 2025; Accepted 28 March 2025
Available online 29 March 2025

upregulation could reflect an increase in the number of TSPO per cell, or a proliferation of cells expressing it. In the human brain, TSPO is overexpressed by astrocytic and microglial cell populations and may reflect alterations in microglia density [7,8,13].

The interest around TSPO lies on the fact that it is essentially the only marker of microglial and astrocytic density that can be measured using in vivo molecular imaging of the human brain. To achieve this objective, a number of TSPO ligands have been developed for use in positron emission tomography (PET) [14]. The first-generation ligand [^{11}C]-PK11195 exhibited limitations in terms of brain uptake, poor specific binding, and elevated non-specific binding. Second-generation ligands have addressed these issues. However, these ligands are susceptible to TSPO polymorphism. Indeed, depending on the extent of binding of second-generation ligands to TSPO, subjects can be classified as high-affinity binders (HAB), mix-affinity binders (MAB), or low-affinity binders (LAB), depending on whether they possess no, one, or two copies of a single polymorphism rs6971 (TSPO Ala147Thr) [15]. Conversely, third-generation ligands seem to combine a high signal-to-noise ratio with insensitivity to TSPO polymorphism [16,17]. For example, in a comparative study between [^{11}C]ER176 and ^{11}C-PBR28 (3rd and 2nd generation ligand, respectively), the [^{11}C]ER176 showed higher time-activity curves and 4 to 9 times greater overall binding than [^{11}C]PBR28, in HAB and MAB subjects, respectively [18].

In order to ensure the safe and effective use of PET in routine clinical practice, it is essential to understand the biodistribution of PET molecules and to determine the radiation dose to which patients are exposed. In the case of [^{18}F]PBR111, a study in one male and one female non-human primate demonstrated rapid clearance, and the estimated effective dose in humans derived from baboon data was determined to be 21 μSv/MBq [19]. In the same study, a calculation of the effective dose from biodistribution data obtained in 16 rats yielded a value of 29 μSv/MBq, which lends support to the monkey estimate but overestimates it [19]. Nevertheless, direct measurements in humans are lacking. Thus, the main aim of our study was to measure the whole-body distribution and dosimetry of [^{18}F]PBR111 in healthy humans.

2. Methods

2.1. Volunteers

Six healthy volunteers (3 females, 3 males) participated in this study. All subjects were free of chronic physical or psychiatric conditions and had not experienced any episode of acute infectious, inflammatory or allergic episode for at least one month prior to the examination. The absence of clinically significant hematological and serum biochemical alterations was confirmed prior to PET imaging. Approval for the study was obtained from the Committee for Medical Ethics of the University Hospitals of Geneva (CE Number: 2022–00542). All participants provided informed consent. The trial registration number is NCT06398392.

2.2. Genotyping

A blood sample was used to extract gDNA using manufacturer protocol. The presence of the rs6971 polymorphism within the TSPO gene was measured by TaqMan SNP genotyping assay (Applied Biosystem). Volunteers were then classified as high affinity binders (HAB, absence of the rs6971 polymorphism) and mixed affinity binders (MAB, heterozygous for this polymorphism). There was no low affinity binder (LAB, homozygous for the rs6971 polymorphism).

2.3. [^{18}F]PBR111 synthesis

The precursor for [^{18}F]PBR111 was purchased from ABX radiopharmaceuticals (Radeberg, Germany, Prod. No. 1657) and stored at −20 °C prior to use. By using an AllInOne module and commercially available reagents (Trasis, Belgium), an automated process for routine synthesis of [^{18}F]PBR111 was developed. [^{18}F]-Fluoride was produced via the ^{18}O(p, n)18F nuclear reaction in a 18.5-MeV IBA cyclotron (~100 GBq starting activity). The aqueous [^{18}F]-fluoride solution in [^{18}O]water was trapped with a resin cartridge (QMA, Waters), eluted with a solution of tetrabutylammonium hydroxide, dried at 110 °C azeotropically, and re-dissolved in anhydrous acetonitrile containing 2 mg of precursor for radiolabeling. After 20 min at 90 °C, the crude was quenched with water then loaded on a semi-preparative HPLC system. Formulation for human injection involved passing the diluted fraction through two prepared C18 SepPak light cartridges (Waters) in series, rinsing with water, eluting with ethanol then saline, and finally passing through a membrane filter. The final prepared dose represented 5–7 GBq with a preparation time of 90 min. Specific activity at the time of injection was 387.70 ± 38.50 MBq/μg (molar activity: 161.7 ± 16.1 GBq/μmol).

2.4. PET and CT acquisition

Dynamic whole-body PET/CT imaging was performed on a Siemens Biograph™ Vision 600 Edge (Siemens Healthineers, Erlangen, Germany) PET/CT scanner at Geneva University Hospitals. Patients received [^{18}F]PBR111, administered as a smooth bolus followed by a 20-ml saline flush through an intravenous catheter placed in the antecubital fossa before scanning. A sequence of 10 dynamic PET scans was acquired immediately post-tracer injection using continuous bed motion (CBM) mode, with ever increasing time intervals: two scans at 8.4 mm/s, two at 4.2 mm/s, two at 2.1 mm/s, one at 1.1 mm/s, one at 0.7 mm/s, and two at 0.5 mm/s. The average total scan time was 132.67 ± 7.76 min, varying based on patient height. Image reconstruction was performed using a 3D iterative ordinary Poisson ordered subset-expectation maximization (OP-OSEM) algorithm with 2 iterations and 21 subsets, integrating TOF 2i5s, resolution modeling, and post-reconstruction Gaussian filtering at 2 mm FWHM. The matrix size was 440 × 440 with a 5-mm slice thickness and pixel spacing of 1.65 × 1.65 mm. Corrections for scatter and attenuation were applied, using model-based scatter scaling for scatter correction and low-dose CT for attenuation correction. Whole-body low-dose CT scans were acquired at 100 kVp, with an average tube current of 162.33 ± 205.79 mA, pitch factors of 0.8 (for two patients) or 1.0 (for four patients), and a 3-mm slice thickness. Data were expressed in SUV Body weight (g/ml) as follows: SUV = (A/D)* W * 1000 with A: activity concentration in the image (Bq/ml), D: injected dose (Bq) and W: weight of the subject (kg).

2.5. Organ dose estimation

Dose estimation was carried out using OLINDA/EXM Version 2.2 [20]. To this end, every 10 PET frames were first decay corrected considering the injection time and PET acquisition time of each frame. Then, volumes of interest, including the heart wall, brain, kidneys, liver, lungs, spleen, bone-marrow, urinary bladder, adrenal glands, gall bladder, pancreas, small intestine, stomach and body contour were segmented using a previously trained deep learning model for organ segmentation [21,22]. All regions with red bone-marrow (such as pelvis, sternum, rib cage, scapula, skull, vertebrae, femur, humerus, etc.) were included in the analysis. An example of the red bone-marrow is given in Supplemental fig. 1. The rest of the body was considered as remainder as no significant activity uptake was observed. The segmented organ masks were subtracted from the body contour to obtain the remainder. Activities percentages within each organ were calculated on every 10 PET frames from dynamic imaging. The activity values, along with their corresponding imaging times, were then input into OLINDA for time-activity curve (TAC) fitting and consequently time-integrated activity and dose calculations. Effective dose calculations are performed in accordance with the International Commission on Radiological Protection (ICRP) recommendations in ICRP-103 [23].

Table 1
Volunteer characteristics. Men have a higher height and mass than women (Unpaired *t*-test: $^{**}p = 0.0022$ and $^{****}p < 0.0001$, respectively).

	Age (years)		Size (cm)		Weight (kg)		Injected activity (MBq)		HAB/MAB
Female	30	± 7.8	163	± 4.0	73	± 1.5	191.71	± 16.15	1/2
Male	27	± 5.6	181	± 1.7**	56	± 0.58****	186.17	± 2.65	3/0
All	29	± 6.3	172	± 10	65	± 9.4	188.94	± 10.79	4/2

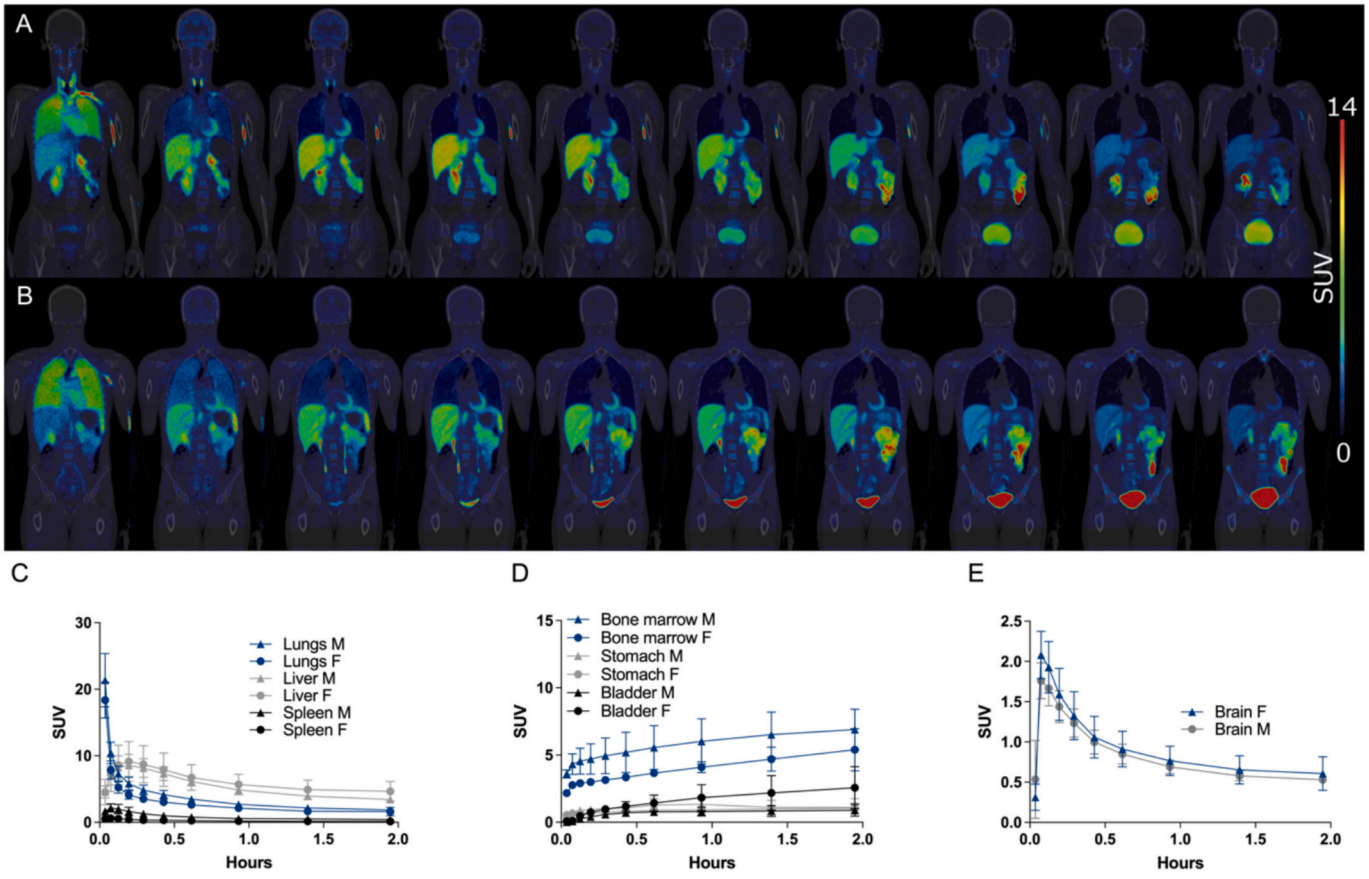

Fig. 1. Whole body distribution of [^{18}F]-PBR111. A-B, Representative images of [^{18}F]PBR111 in a female (A) and male (B) healthy subject. Images were decay corrected, coregistred to the CT scan and expressed in SUV. C—D, Time-activity curves (SUV body weight, g/ml) in representative organs showing either decreased (C) or increased (D) [^{18}F]PBR111 levels overtime. E, Mean time-activity curves and individual dots [^{18}F]PBR111 levels in the brain of females (grey) and males (black). M: male, F: female.

2.6. Statistical analysis

From the time-activity curves, area under curves (AUC) were estimated for each organ. The Mann-Whitney test with the FDR correction for multiple testing was used to analyze AUC with the sex as factor. The Friedman test with the Dunn's multiple comparisons test was used to analyze the dose received by organs and the contribution to the effective doses from each organ, with GraphPad Prism 10. Data are presented as mean ± SD.

3. Results

Data on age, sex, polymorphism and doses injected are given in Table 1. Both groups received similar doses of [^{18}F]PBR111 (around 200 MBq). Representative images of [^{18}F]PBR111 tracking over time in the whole body of a female and a male participant are shown in Fig. 1A-B. It appears that some organs accumulate radioactivity, while others show decreasing levels over time. These observations were confirmed by measurements of the time course of radioactivity, as shown in Fig. 1C-E for the main organs (the full set of measurements are presented in Supplemental table 1). The [^{18}F]PBR111 dose (expressed in SUV) showed a peak value in the lungs (19.87 ± 3.47 considering the 6 volunteers) at $t = 2$ min, and in the liver (8.85 ± 2.19) at $t = 12$ min. The other organs such as the brain (1.91 ± 0.29) and the heart wall (0.393 ± 0.05) showed low radioactivity levels. In contrast to organs showing a decrease in radioactivity over time, an accumulation of [^{18}F]PBR111 was observed over time in the bone marrow (6.14 ± 1.6), the bladder (1.73 ± 1.38; and the gall-bladder: 0.14 ± 0.11), and the stomach (1.07 ± 0.48) at $t = 120$ min. The areas under the curve calculated for all the organs showed no significant differences between males and females (Mann-Whitney tests). In addition, the [^{18}F]PBR111 kinetics do not seem to differ between HAB and MAB subjects (Supplemental Fig. 2).

In the brain, an analysis of different regions was carried out. Fig. 2 shows a representative example of the [^{18}F]PBR111 accumulation in the brain and quantitative data in some areas showing the dynamics of [^{18}F]PBR111. Interestingly, the skull shows an accumulation of [^{18}F]PBR111, which could suggest defluorination.

The dose received by organs and the contribution to the effective doses from each organ are given in Table 2. Statistical analysis showed that the [^{18}F]PBR111 accumulation did not depend on the sex of the

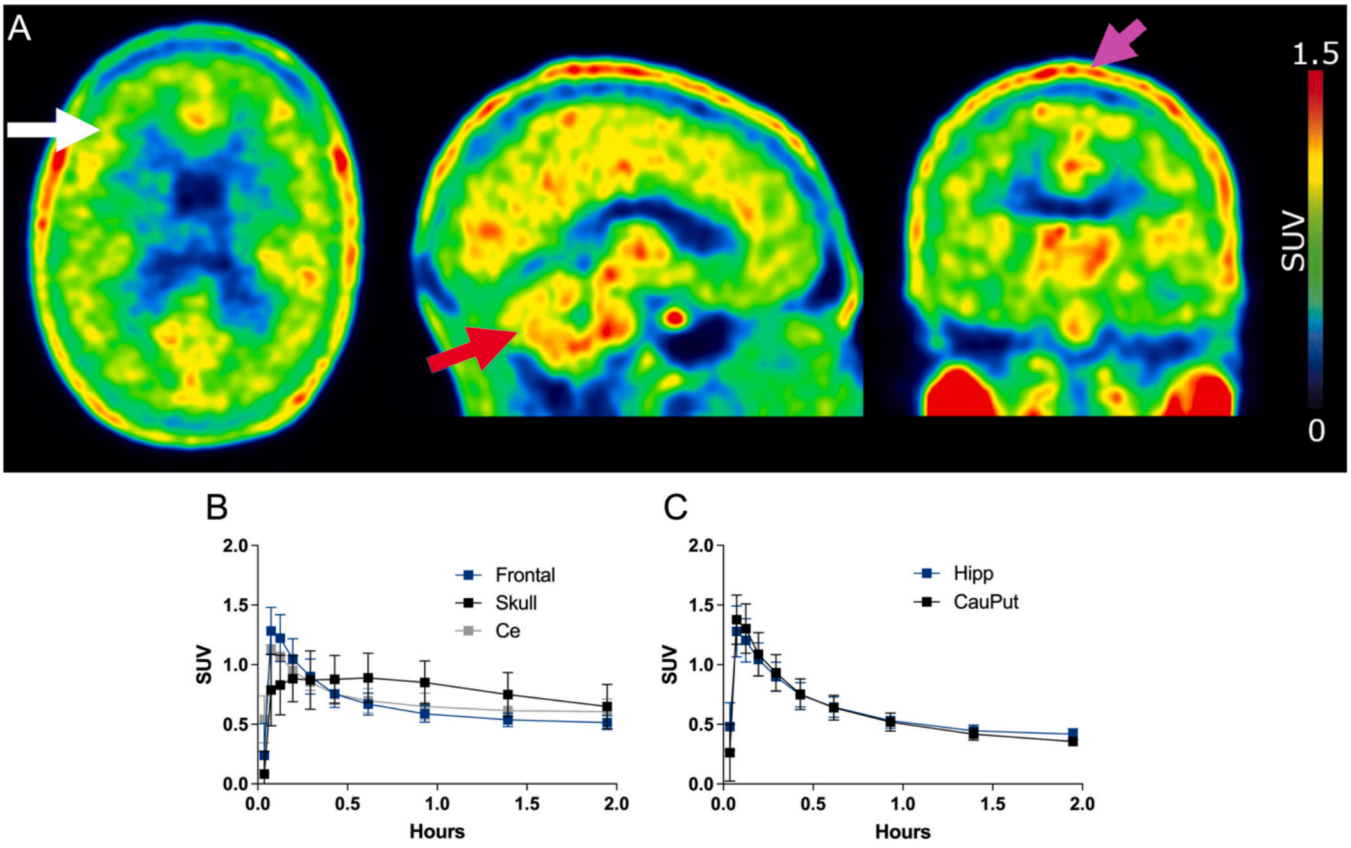

Fig. 2. Brain distribution of [^{18}F]-PBR111. A, Representative images of [^{18}F]PBR111 accumulation in a male healthy subject. Some brain areas are identified by arrows: frontal cortex (white), cerebellum (red), and the skull (pink). B—C, Time-activity curves (SUV body weight, g/ml) of [^{18}F]PBR111 levels in representative brain areas. Abbreviations: CauPut: caudate/putamen, Ce: cerebellum, Hipp: hippocampus. (For interpretation of the references to colour in this figure legend, the reader is referred to the web version of this article.)

Table 2
Organ Doses (μSv/MBq) and effective doses (μSv/ MBq).

	Organe doses (μSv/MBq)						Effective Doses (μSv/ MBq)					
	Male ±*SD*		Fem. ±*SD*		All ±*SD*		Male ±*SD*		Fem. ±*SD*		All ±*SD*	
Adrenals	25.20	*17.05*	18.50	*5.72*	21.85	*11.95*	0.23	*0.16*	0.17	*0.05*	0.20	*0.11*
Brain	5.09	*0.13*	7.48	*1.58*	6.29	*1.65*	0.05	*0.00*	0.07	*0.02*	0.06	*0.02*
Esophagus	9.85	*1.43*	11.02	*1.53*	10.44	*1.47*	0.39	*0.06*	0.44	*0.06*	0.42	*0.06*
Eyes	4.68	*0.46*	6.51	*0.65*	5.59	*1.12*	0.00	*0.00*	0.00	*0.00*	0.00	*0.00*
Gallbladder wall	14.77	*1.87*	19.73	*2.69*	17.25	*3.42*	0.14	*0.02*	0.18	*0.02*	0.16	*0.03*
left colon	12.67	*1.93*	12.40	*1.44*	12.53	*1.53*	0.61	*0.09*	0.60	*0.07*	0.61	*0.07*
Small Intestine	38.50	*2.08*	42.87	*21.89*	40.68	*14.11*	0.36	*0.02*	0.40	*0.20*	0.38	*0.13*
Stomach Wall	24.27	*4.99*	27.53	*5.59*	25.90	*5.07*	2.91	*0.61*	3.30	*0.67*	3.11	*0.61*
Right colon	10.17	*1.24*	11.83	*1.31*	11.00	*1.46*	0.49	*0.06*	0.57	*0.06*	0.53	*0.07*
Rectum	8.51	*0.42*	12.20	*1.65*	10.36	*2.29*	0.20	*0.01*	0.28	*0.04*	0.24	*0.05*
Heart Wall	12.50	*0.98*	14.80	*1.75*	13.65	*1.79*	0.12	*0.01*	0.14	*0.02*	0.13	*0.02*
Kidneys	113.5	*153.7*	28.87	*13.28*	71.18	*108.0*	1.05	*1.42*	0.27	*0.12*	0.66	*1.00*
Liver	24.37	*3.11*	41.00	*10.31*	32.68	*11.38*	0.97	*0.12*	1.64	*0.41*	1.31	*0.45*
Lungs	26.20	*15.35*	22.10	*4.48*	24.15	*10.36*	3.15	*1.83*	2.65	*0.54*	2.90	*1.24*
Pancreas	24.47	*2.36*	23.63	*7.05*	24.05	*4.72*	0.23	*0.02*	0.22	*0.07*	0.22	*0.04*
Salivary glands	5.42	*0.52*	6.86	*0.72*	6.14	*0.97*	0.05	*0.01*	0.07	*0.01*	0.06	*0.01*
Red Marrow	19.83	*3.59*	22.77	*2.01*	21.30	*3.06*	2.38	*0.43*	2.73	*0.24*	2.56	*0.37*
Osteogenic Cells	13.80	*2.00*	14.17	*1.25*	13.98	*1.50*	0.14	*0.02*	0.14	*0.01*	0.14	*0.02*
Spleen	35.67	*10.71*	25.37	*12.34*	30.52	*11.78*	0.33	*0.10*	0.23	*0.11*	0.28	*0.11*
Thymus	7.94	*1.25*	9.96	*1.28*	8.95	*1.58*	0.07	*0.01*	0.09	*0.01*	0.08	*0.01*
Thyroid	7.01	*1.08*	7.86	*0.99*	7.43	*1.04*	0.28	*0.04*	0.31	*0.04*	0.30	*0.04*
Urinary Bladder Wall	15.47	*1.15*	37.67	*13.05*	26.57	*14.71*	0.62	*0.05*	1.51	*0.52*	1.06	*0.59*
Prostate	7.69	*0.55*	–	–	7.69	*0.55*	0.04	*0.00*	–	–	0.04	*0.00*
Testes	4.95	*0.58*	–	–	4.95	*0.58*	0.20	*0.02*	–	–	0.20	*0.02*
Breasts	–	–	6.96	*0.80*	6.96	*0.80*	–	–	0.84	*0.10*	0.84	*0.10*
Ovaries	–	–	11.47	*1.17*	11.47	*1.17*	–	–	0.46	*0.05*	0.45	*0.05*
Uterus	–	–	13.03	*2.02*	13.03	*2.02*	–	–	0.06	*0.01*	0.06	*0.01*
Whole body	7.97	*0.57*	10.51	*1.24*	9.24	*1.64*	14.97	*2.16*	17.37	*2.81*	16.17	*2.60*

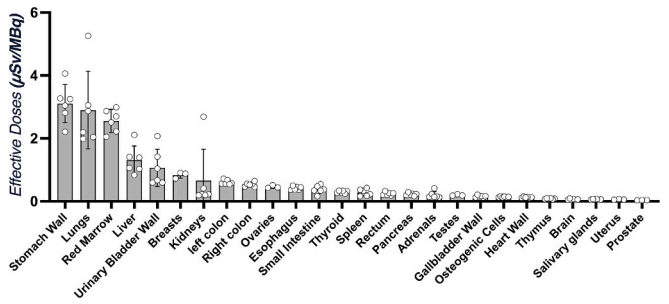

Fig. 3. Contribution to the effective doses (µSv/MBq) from each organ. From left to right, organs are arranged based on their relative contribution to the effective dose, as defined by ICRP-103.

individual (Mann-Whitney tests). The Friedman test applied on all subjects showed that the effective doses is dependent of the organ ($\chi^2(20) = 112.7, p < 0.0001$). Stomach, lungs and red marrow absorbed more radioactivity, liver showed intermediate levels, and the other organs absorbed less radioactivity (Fig. 3). The total effective dose was 16.17 ± 2.60 µSv/MBq. Healthy volunteers were exposed to 3.04 ± 0.46 mSv following a [^{18}F]PBR111 injection at 188.94 MBq. The time integrated activities in organs (MBq.h/MBq) are given in Table 3.

4. Discussion

Our study is the first to measure [^{18}F]PBR111 dosimetry in human. We show that overall, men and women have similar accumulation profiles. Interestingly, while the monkey estimate was 27 % lower than that based on rat data, the actual human data is 23 % and 44 % lower than the monkey and rat estimates, respectively [19]. Predictive models therefore overestimate the dose to which subjects are exposed.

Among the interests of in vivo quantification of TSPO in humans, studies of psychiatric and neurodegenerative diseases have largely focused on this marker to demonstrate the presence of cerebral neuroinflammatory reactions. [^{18}F]PBR111 has been widely employed in previous clinical studies [24,26–30]. Notably, Ottoy et al. (2018) demonstrated that [^{18}F]PBR111 exhibits moderate test–retest variability (16–22 %) and good reliability, making it a robust radioligand for TSPO imaging [30]. Additionally, studies have shown that [^{18}F]PBR111 binding kinetics can be reliably quantified using an advanced pharmacokinetic model, which accounts for vascular trapping and improves the accuracy of TSPO quantification [30]. One possible limitation associated to the use of [^{18}F]PBR111 is its presence in the skull that could interfere with the measurement in adjacent brain areas (spill-over effect), as previously suggested [24,25]. [^{18}F]PBR111 defluorination has also been suggested by its accumulation in bone marrow. However, this defluorination component does not prevent quantification. Indeed, the defluorination component and its effect on structures adjacent to skull can be corrected using modeling techniques or techniques based on factor analysis [31].We also observed accumulation in the stomach, which could be relevant for future studies assessing the density of myeloid cells in the digestive tract in relationship to their density in the CNS as previously suggested in a study assessing TSPO density in the digestive system of an Alzheimer's disease rat model [7].

To compare with other TSPO ligands, we considered human data for [^{18}F]-PBR06, [^{18}F]-FEPPA and [^{18}F]-FEDAA1106 [32–34]. Overall, the behavior of [^{18}F]PBR111 in the body is similar to that of other radioligands. It appears that the gallbladder wall is more affected by [^{18}F]-PBR06 (367.0 µSv/MBq) as compared to the other radioligands ([^{18}F]PBR111: 17.25 µSv/MBq; [^{18}F]FEPPA: 16.1 µSv/MBq and [^{18}F]FEDAA1106: 27 µSv/MBq). In addition, the small intestine and stomach wall receive more radiation exposure with [^{18}F]-FEDAA1106 (60 and 40 µSv/MBq) and [^{18}F]PBR111 (40.68 and 25.9 µSv/MBq) than with [^{18}F]-FEPPA (11.8 and 12.9 µSv/MBq) and [^{18}F]-PBR06 (13.3 and 13.0 µSv/MBq). However, [^{18}F]PBR111 show low levels than [^{18}F]-FEDAA1106 in thyroid (7.4 vs 59 µSv/MBq, respectively), spleen (30.5 vs 120 µSv/MBq), lungs (24.1 vs 82 µSv/MBq) and heart wall (13.6 vs 48 µSv/MBq). Thus, exposure data are relatively close, with a few variations undoubtedly linked to the physicochemical nature of the ligands. Overall, the patient's radiation exposure with [^{18}F]PBR111 (total effective dose:16.17 µSv/MBq) is of the same order as that of the previous studies ([^{18}F]-PBR06: 18.5 µSv/MBq; [^{18}F]-FEPPA: 21.0 µSv/MBq and [^{18}F]-FEDAA1106: 36 µSv/MBq).

Thus, whole body distribution and dosimetry data of [^{18}F]PBR111 are compatible with its use in clinical research protocols. This study performed personalized dosimetry for the newly developed radiopharmaceutical, this information is valuable for justification and optimization purposes. The knowledge about the organ dose and effective radiation dose is key for justified investigations and informed decisions taking into account the radiation risk.

CRediT authorship contribution statement

Benjamin B. Tournier: Writing – original draft, Validation, Funding acquisition, Formal analysis, Conceptualization. **Zahra Mansouri:** Writing – review & editing, Methodology, Formal analysis. **Yazdan Salimi:** Writing – review & editing, Methodology, Formal analysis. **Kelly Ceyzériat:** Writing – review & editing. **Gregory Mathoux:** Writing – review & editing, Investigation. **Hélène Richard-Lepouriel:** Writing – review & editing, Investigation. **Daniel Zullino:** Writing – review & editing. **Frédéric Bois:** Writing – review & editing, Methodology. **Habib Zaidi:** Writing – review & editing, Methodology, Formal analysis. **Valentina Garibotto:** Writing – review & editing, Investigation. **Stergios Tsartsalis:** Writing – original draft, Validation, Supervision, Investigation, Funding acquisition, Conceptualization. **Philippe Millet:** Writing – original draft, Validation, Supervision, Funding

Table 3
Time integrated activities (MBq.h/MBq).

	Male ±*SD*		Fem. ±*SD*		All ±*SD*	
Adrenals	3.70E-04	*9.54E-05*	1.57E-04	*1.50E-04*	2.63E-04	*1.62E-04*
Brain	2.72E-02	*1.01E-02*	2.44E-02	*4.33E-03*	2.58E-02	*7.14E-03*
Gallbladder wall	7.33E-04	*4.93E-04*	3.21E-03	*1.83E-03*	1.97E-03	*1.81E-03*
Small intestine	1.24E-01	*8.96E-03*	9.84E-02	*6.83E-02*	1.11E-01	*4.58E-02*
Stomach wall	4.44E-02	*3.15E-03*	2.81E-02	*7.45E-03*	3.62E-02	*1.03E-02*
Heart wall	9.20E-03	*1.81E-03*	9.40E-03	*2.55E-03*	9.30E-03	*1.98E-03*
Kidneys	3.77E-02	*1.18E-02*	1.74E-01	*2.67E-01*	1.06E-01	*1.85E-01*
Liver	1.92E-01	*8.47E-02*	1.68E-01	*3.00E-02*	1.80E-01	*5.84E-02*
Lungs	1.54E-01	*1.10E-01*	9.08E-02	*2.30E-02*	1.22E-01	*7.87E-02*
Pancreas	1.14E-02	*9.54E-04*	6.17E-03	*1.20E-03*	8.78E-03	*3.03E-03*
Red marrow	1.67E-01	*1.25E-02*	1.87E-01	*4.98E-02*	1.77E-01	*3.42E-02*
Spleen	2.08E-02	*4.72E-03*	1.42E-02	*1.07E-02*	1.75E-02	*8.25E-03*
Urinary bladder wall	3.79E-02	*3.49E-02*	3.55E-02	*1.44E-02*	3.67E-02	*2.39E-02*
Whole body	1.01E+00	*1.13E-01*	9.46E-01	*1.77E-01*	9.78E-01	*1.37E-01*

acquisition, Conceptualization.

Funding

This work was supported by the Swiss National Science Foundation (no. 320030-184713) and the University Hospitals of Geneva (Research and Development Program 10-2018-I and 17-2018-I).

Declaration of competing interest

The authors declare that they have no conflict of interest.

Acknowledgments

With contributions of the Clinical Research Center, University Hospital and Faculty of Medicine, Geneva. We also thank Mme Anne Viala, Mme Anne-Charlotte Paporé and Mr. Jean-Baptiste Richard for expert assistance with the clinical and laboratory assessments.

Appendix A. Supplementary data

Supplementary data to this article can be found online at https://doi.org/10.1016/j.nucmedbio.2025.109011.

References

[1] Betlazar C, Harrison-Brown M, Middleton RJ, Banati R, Liu GJ. Cellular sources and regional variations in the expression of the Neuroinflammatory marker translocator protein (TSPO) in the Normal brain. Int J Mol Sci 2018;19.
[2] Gui Y, Marks JD, Das S, Hyman BT, Serrano-Pozo A. Characterization of the 18 kDa translocator protein (TSPO) expression in post-mortem normal and Alzheimer's disease brains. Brain Pathol 2020;30:151–64.
[3] Guilarte TR, Rodichkin AN, McGlothan JL, Acanda De La Rocha AM, Azzam DJ. Imaging neuroinflammation with TSPO: a new perspective on the cellular sources and subcellular localization. Pharmacol Ther 2022;234:108048.
[4] Banati RB, Newcombe J, Gunn RN, Cagnin A, Turkheimer F, Heppner F, et al. The peripheral benzodiazepine binding site in the brain in multiple sclerosis: quantitative in vivo imaging of microglia as a measure of disease activity. Brain 2000;123(Pt 11):2321–37.
[5] Nack A, Brendel M, Nedelcu J, Daerr M, Nyamoya S, Beyer C, et al. Expression of translocator protein and [18F]-GE180 ligand uptake in multiple sclerosis animal models. Cells 2019:8.
[6] Zinnhardt B, Belloy M, Fricke IB, Orije J, Guglielmetti C, Hermann S, et al. Molecular imaging of immune cell dynamics during De- and Remyelination in the Cuprizone model of multiple sclerosis by [(18)F]DPA-714 PET and MRI. Theranostics 2019;9:1523–37.
[7] Tournier BB, Tsartsalis S, Ceyzeriat K, Fraser BH, Gregoire MC, Kovari E, et al. Astrocytic TSPO upregulation appears before microglial TSPO in Alzheimer's disease. J Alzheimers Dis 2020;77:1043–56.
[8] Tournier BB, Tsartsalis S, Ceyzeriat K, Medina Z, Fraser BH, Gregoire MC, et al. Fluorescence-activated cell sorting to reveal the cell origin of radioligand binding. J Cereb Blood Flow Metab 2020;40:1242–55.
[9] Qin L, Xiao L, Zhu H, Du Y, Tang Y, Feng L. Translocator protein (18 kDa) positron emission tomography imaging as a biomarker of neuroinflammation in epilepsy. Neurol Sci 2024;45:5201–11.
[10] De Picker LJ, Morrens M, Branchi I, Haarman BCM, Terada T, Kang MS, et al. TSPO PET brain inflammation imaging: a transdiagnostic systematic review and meta-analysis of 156 case-control studies. Brain Behav Immun 2023;113:415–31.
[11] van Kesteren CF, Gremmels H, de Witte LD, Hol EM, Van Gool AR, Falkai PG, et al. Immune involvement in the pathogenesis of schizophrenia: a meta-analysis on postmortem brain studies. Transl Psychiatry 2017;7:e1075.
[12] Plaven-Sigray P, Matheson GJ, Collste K, Ashok AH, Coughlin JM, Howes OD, et al. Positron emission tomography studies of the glial cell marker translocator protein in patients with psychosis: a Meta-analysis using individual participant data. Biol Psychiatry 2018;84:433–42.
[13] Nutma E, Fancy N, Weinert M, Tsartsalis S, Marzin MC, Muirhead RCJ, et al. Translocator protein is a marker of activated microglia in rodent models but not human neurodegenerative diseases. Nat Commun 2023;14:5247.
[14] Salerno S, Viviano M, Baglini E, Poggetti V, Giorgini D, Castagnoli J, et al. TSPO Radioligands for Neuroinflammation: an overview. Molecules 2024;29:4212.
[15] Owen DR, Gunn RN, Rabiner EA, Bennacef I, Fujita M, Kreisl WC, et al. Mixed-affinity binding in humans with 18-kDa translocator protein ligands. J Nucl Med 2011;52:24–32.
[16] Lee N, Choi JY, Ryu YH. The development status of PET radiotracers for evaluating neuroinflammation. Nucl Med Mol Imaging 2024;58:160–76.
[17] Salerno S, Viviano M, Baglini E, Poggetti V, Giorgini D, Castagnoli J, et al. TSPO Radioligands for Neuroinflammation: an overview. Molecules 2024;29.
[18] Zanotti-Fregonara P, Pascual B, Veronese M, Yu M, Beers D, Appel SH, et al. Head-to-head comparison of (11)C-PBR28 and (11)C-ER176 for quantification of the translocator protein in the human brain. Eur J Nucl Med Mol Imaging 2019;46:1822–9.
[19] Verschuer JD, Towson J, Eberl S, Katsifis A, Henderson D, Lam P, et al. Radiation dosimetry of the translocator protein ligands [18F]PBR111 and [18F]PBR102. Nucl Med Biol 2012;39:742–53.
[20] Stabin MG. OLINDA/EXM 2-the next-generation personal computer software for internal dose assessment in nuclear medicine. Health Phys 2023;124:397–406.
[21] Salimi Y, Shiri I, Mansouri Z, and Zaidi H. Deep learning-assisted multiple organ segmentation from whole-body CT images. medRxiv 2023:2023.10.20.23297331.
[22] Salimi Y, Mansouri Z, Shiri I, Mainta I, and Zaidi H. Deep Learning-powered CT-less Multi-tracer Organ Segmentation from PET Images: A solution for unreliable CT segmentation in PET/CT Imaging. medRxiv 2024:2024.08.27.24312482.
[23] The 2007 Recommendations of the International Commission on Radiological Protection. ICRP publication 103. Ann ICRP 2007;37:1–332.
[24] Guo Q, Colasanti A, Owen DR, Onega M, Kamalakaran A, Bennacef I, et al. Quantification of the specific translocator protein signal of 18F-PBR111 in healthy humans: a genetic polymorphism effect on in vivo binding. J Nucl Med 2013;54:1915–23.
[25] Fookes CJ, Pham TQ, Mattner F, Greguric I, Loc'h C, Liu X, et al. Synthesis and biological evaluation of substituted [18F]imidazo[1,2-a]pyridines and [18F]pyrazolo[1,5-a]pyrimidines for the study of the peripheral benzodiazepine receptor using positron emission tomography. J Med Chem 2008;51:3700–12.
[26] Colasanti A, Guo Q, Giannetti P, Wall MB, Newbould RD, Bishop C, et al. Hippocampal Neuroinflammation, functional connectivity, and depressive symptoms in multiple sclerosis. Biol Psychiatry 2016;80:62–72.
[27] Colasanti A, Guo Q, Muhlert N, Giannetti P, Onega M, Newbould RD, et al. In vivo assessment of brain white matter inflammation in multiple sclerosis with (18)F-PBR111 PET. J Nucl Med 2014;55:1112–8.
[28] De Picker L, Ottoy J, Deleye S, Verhaeghe J, Stroobants S, Wyffels L, et al. Test–retest reliability of [18F]PBR111 binding to translocator protein (TSPO) in young healthy control subjects. Eur Neuropsychopharmacol 2016;26:S214.
[29] De Picker L, Ottoy J, Verhaeghe J, Deleye S, Wyffels L, Fransen E, et al. State-associated changes in longitudinal [(18)F]-PBR111 TSPO PET imaging of psychosis patients: evidence for the accelerated ageing hypothesis? Brain Behav Immun 2019;77:46–54.
[30] Ottoy J, De Picker L, Verhaeghe J, Deleye S, Wyffels L, Kosten L, et al. (18)F-PBR111 PET imaging in healthy controls and schizophrenia: test-retest reproducibility and quantification of Neuroinflammation. J Nucl Med 2018;59:1267–74.
[31] Millet P, Moulin-Sallanon M, Tournier BB, Dumas N, Charnay Y, Ibanez V, et al. Quantification of dopamine D(2/3) receptors in rat brain using factor analysis corrected [18F]Fallypride images. Neuroimage 2012;62:1455–68.
[32] Fujimura Y, Kimura Y, Simeon FG, Dickstein LP, Pike VW, Innis RB, et al. Biodistribution and radiation dosimetry in humans of a new PET ligand, (18)F-PBR06, to image translocator protein (18 kDa). J Nucl Med 2010;51:145–9.
[33] Mizrahi R, Rusjan PM, Vitcu I, Ng A, Wilson AA, Houle S, et al. Whole body biodistribution and radiation dosimetry in humans of a new PET ligand, [(18)F]-FEPPA, to image translocator protein (18 kDa). Mol Imaging Biol 2013;15:353–9.
[34] Takano A, Gulyas B, Varrone A, Karlsson P, Sjoholm N, Larsson S, et al. Biodistribution and radiation dosimetry of the 18 kDa translocator protein (TSPO) radioligand [18F]FEDAA1106: a human whole-body PET study. Eur J Nucl Med Mol Imaging 2011;38:2058–65.